Numerical and Experimental Investigation of Laser-induced Optoacoustic Wave Propagation for Damage Detection

by

Chen Liu

A Thesis Presented in Partial Fulfillment
of the Requirements for the Degree
Master of Science

Approved July 2016 by the
Graduate Supervisory Committee:

Yongming Liu, Chair
Liping Wang
Yang Jiao

ARIZONA STATE UNIVERISTY

August 2016

ABSTRACT

An integrated experimental and numerical investigation for laser-generated optoacoustic wave propagation in structural materials is performed. First, a multi-physics simulation model is proposed to simulate the pulsed laser as a point heat source which hits the surface of an aluminum sheet. The pulsed laser source can generate a localized heating on the surface of the plate and induce an in-plane stress wave. ANSYS – a finite element analysis software – is used to build the 3D model and a coupled thermal-mechanical simulation is performed in which the heat flux is determined by an empirical laser-heat conversion relationship. The displacement and stress field-histories are obtained to get the time of arrival and wave propagation speed of the stress wave. The effect of an added point mass is investigated in detail to observe the local material perturbation and remote wave signals. Following this, the experimental investigation of optoacoustic wave is also performed. A new experimental setup and control is developed and assembled in-house. Various laser firing parameters are investigated experimentally and the optimal combination is used for the experimental testing. Matrix design for different testing conditions is also proposed to include the effect of wave path, sampling procedure, and local point mass on the optoacoustic wave propagation. The developed numerical simulation results are validated with experimental observations. It is shown that the proposed experimental setup can offer a potential fast scanning method for damage detection (local property change) for plate-like structural component.

DEDICATION

To my dear parents

ACKNOWLEDGMENTS

My deepest gratitude is to my thesis advisor Dr. Yongming Liu for the continuous support of my study and research throughout my Master's period. His patience and guidance helped me to overcome a lot of difficulties and finish this thesis.

I would also like to thank my committee members: Dr. Liping Wang and Dr. Yang Jiao, for their insightful comments and questions.

Last but not the least, my sincere thank goes to my fellow labmates in Arizona State University, especially to Tishun Peng, for enlightening me with the help of the experiment and simulation.

TABLE OF CONTENTS

Page

CHAPTER Page

LIST OF TABLES

Table Page

LIST OF FIGURES

Figure Page

Figure Page

Chapter 1

INTRODUCTION

Cracks exist in various different kinds of materials, such as wood, concrete, metal and composite materials. Many researches focus on the crack behavior of metals among which aluminum and steel are the most common metals used in structures. Cracks in rail, aircraft, and some heavy-duty machines are not easy to be detected directly by employing traditional methods. For instance, attaching sensors to structures may be prohibited due to very expensive cost and due to regulations. Non-contact non-destructive evaluation (NDE) methods are widely used and have been extensively studies in the past. Among them, the wave-based method (e.g., Lamb wave or acoustic wave) is one of the most widely used NDE method due to its high resolution and relatively easy setup. The proposed study is trying to develop a new laser-induced optoacoustic wave propagation model for future implementation for NDE of structural damages. A brief review of the wave-based NDE testing method and simulation models is given below.

1.1 Application of laser scanning technology

Wave-based damage detection methods may be classified into several categories depending on their wave generation and collection methods. The first one is the method that uses sensors to be the excitation and receiving terminals. The sensors are directly glued on the surface of the specimen and the disadvantage of this method is that the sensors on the structure may be damaged during the operation and it is expensive to apply if the structure is very large, such as aircrafts and buildings. A network of the sensors and feature extraction by signal processing are used to do the damage growth monitoring and early

damage detection in the aircraft structure [1]. Lamb wave based method is used to detect geometry and location of the defects, as well as implement wave propagation profile to do the tomography in aluminum plate[2]. Two baseline-free damage detection techniques are compared by using piezoceramic transducers based on the lamb wave based method[3]. Different fiber optic sensors are used to detect the damage for the composite laminate materials based on guided wave[4]. The second approach is the method that uses sensor actuator as the excitation terminal, but the receiving terminal is changed to noncontact laser beams. For example, piezoelectric transducers are used to be the excitation terminal and Laser scanning vibrometers are used to be the receiving terminal in some existing studies[5][6][7]. An alternative way is to use the pulsed laser shooting on the surface of the specimen to generate the wave. The laser beam is absorbed by the small volume of the specimen. The rapid absorption of the laser energy will create a localized heating which results in the expansion of the structure and induces an in-plane stress wave. In the research which employs laser into the experiment[8], the pulsed laser beam is the emission terminal and an electromagnetic acoustic transducer (EMAT) is the received terminal. A new measurement system is developed for generating thermal-excitation ultrasonic signals, a reception transducer receiving signals which generated by a scanning pulsed laser[9]. It should be noted that laser scanning vibrometer can be used to be the receiving terminal. When doing the damage detection, two laser terminal directly shot on the detection area and scanning. This technology is applied on the nuclear industry as presented in the paper[10]. Very small cracks which have the depth of less than 0.1mm can be detected using this method, and there is no need to attach transducers and sensors to the surface of the structure, espe-

cially large structure like aircrafts, tall buildings and bridges. Also, this technology is applied on the new developed composites materials to check their durability and worthiness[11]. The benefits of this approach contains that it can save much time, money and labor.

The proposed study focused on the laser generation of acoustic waves for damage detection. The receiving terminal is attached piezo sensor. There are two main reasons for this: (1) the current lab facilities does not allow non-contact measurements; (2) attached piezo sensor has lower noise and higher signal to noise ratio. One unique component of the proposed study is to use the high frequency MOPA laser compared to most existing studies that employs the YAG laser[12][13][14]. YAG laser usually has high power density and low repetition frequency (10~20 Hz). The MOPA laser usually has lower power density and high repetition rate that is more suitable for large area scanning in the future implementation for damage detection of large structures.

1.2 Application of numerical computational technology

Many numerical computational techniques are developed for wave propagation studies, one of them[15] uses local interaction simulation approach to model a sharp interfaces and discontinuities in complex media, and reports numerical investigations of Lamb wave propagation modelling for damage detection in metallic structures. A more advanced method[16] was used to detect the damage of the structure, in this method, both the emitting terminal and receiving terminal were all non-contacted, laser emission ultrasound wave and generate a stress wave, an infrared camera detect the change of a thermal spot shape of the specimen, this technology is more applicable and efficient in real life because it saves

much time and labor. The thermos-elastic finite element model of laser generation ultrasound was developed and indicated that the laser-generated surface-acoustic waves with high frequencies will be affected by the temperature dependence of the thermos-physical parameters significantly[17]. Based on the laser scanning test, finite element simulation is implemented to validate the reliability of the test[18][19][20]. Also, The laser firing parameters influence the results, in order to get the best combinations, the parametric investigation is needed, using simulation to study how does the laser parameters such as beam radius and rise time influence the ultrasound waves[21]. This study will give a good guideline to the selection of the experimental parameters in the laser testing.

Many researches focus on the thermo-elastic expansion technology applied on detecting cracks and damages of the structures. In this paper, laser detection was used to detect the crack of a metal plate, an electromagnetic acoustic transducer was used to receive signal. ANSYS finite element software built a model and analyze the change of displacement and stress field, according the results of the finite element analysis, compute the time of arrival of stress wave.

Chapter 2

NUMERICAL INVESTIGATION USING FINITE ELEMNT METHOD

This chapter focuses on the numerical simulation using coupled thermos-mechanical analysis for the laser-induced acoustic wave propagation. Model development and parametric studies are investigated in detail. Experimental testing results in chapter 3 will be used to validate the proposed methodology. Details are shown below.

2.1 Finite element model development

Similar methodologies for the finite element simulation have been developed in [22], [23]. The proposed study uses the developed methods to analyze the experimental testing in the proposed study. This model is based on the entity model of the laser testing. The dimension of the specimen and distance between laser beam and sensor are measured from the experimental testing model (details in Chapter 3). The specimen is an aluminum plate and has the height of 0.3048m and width of 0.111125m (Fig. 1). On the upper side of the plate, there are two circles which are set as sensors. Damage is located at 0.0762m away from the top surface of the plate and is represented by a certain number of magnets. The shape of magnets is solid cylinder. Laser beam will shoot on the lower side of the plate and it is set as a solid circle with small radius. Two different directions of laser beam shooting paths are built: one is vertical the other is horizontal (see Fig. 1). In the vertical laser beam path, the distance between the two positions is 0.0254m. In the horizontal laser beam path, the distance is 0.0127m between the two positions.

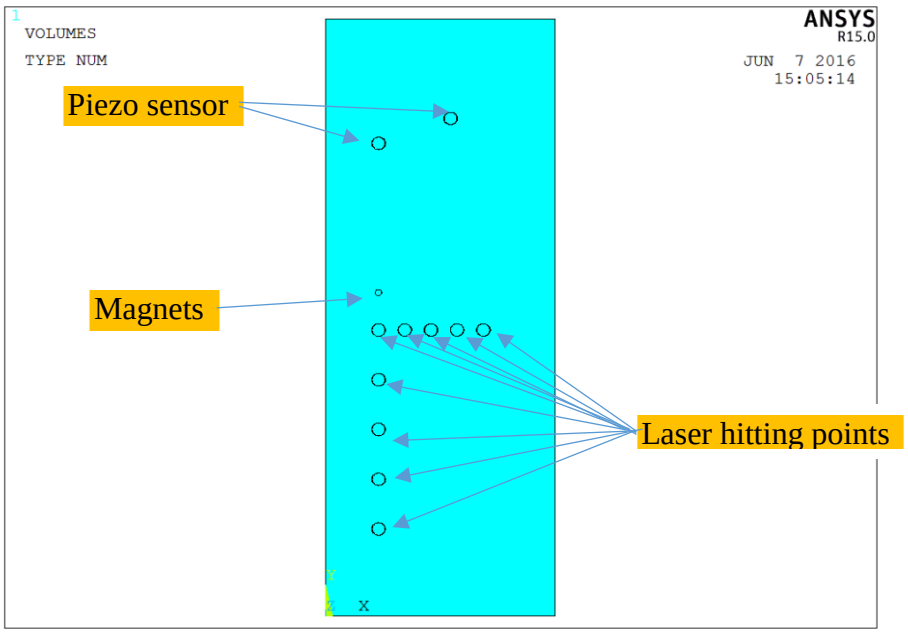
1
VOLUMES
TYPE NUM
ANSYS
R15.0
JUN 7 2016
15:05:14
Piezo sensor
Magnets
Laser hitting points
Y
Z
X

(a)

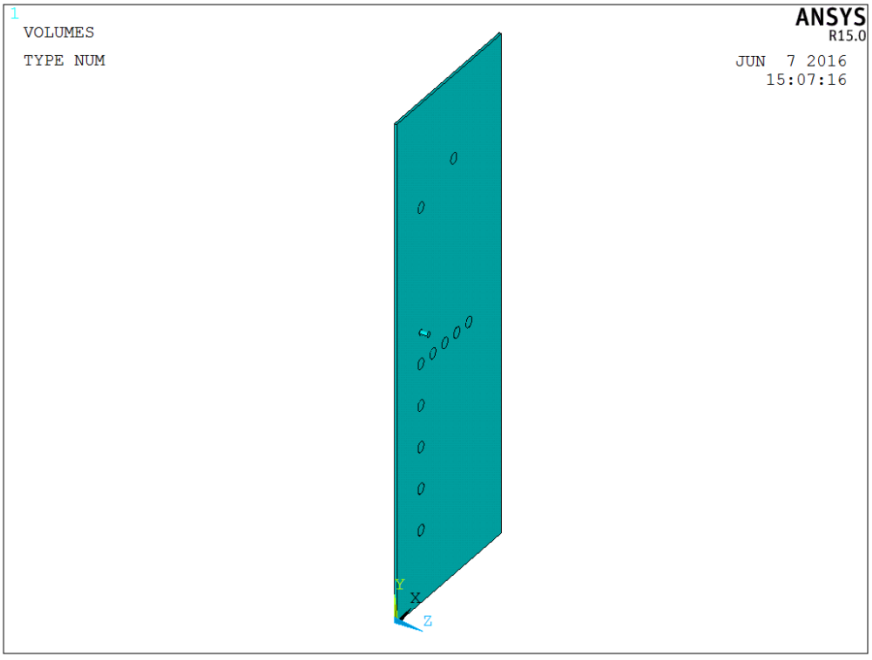
1
VOLUMES
TYPE NUM
ANSYS
R15.0
JUN 7 2016
15:07:16
Y
X
Z

(b)

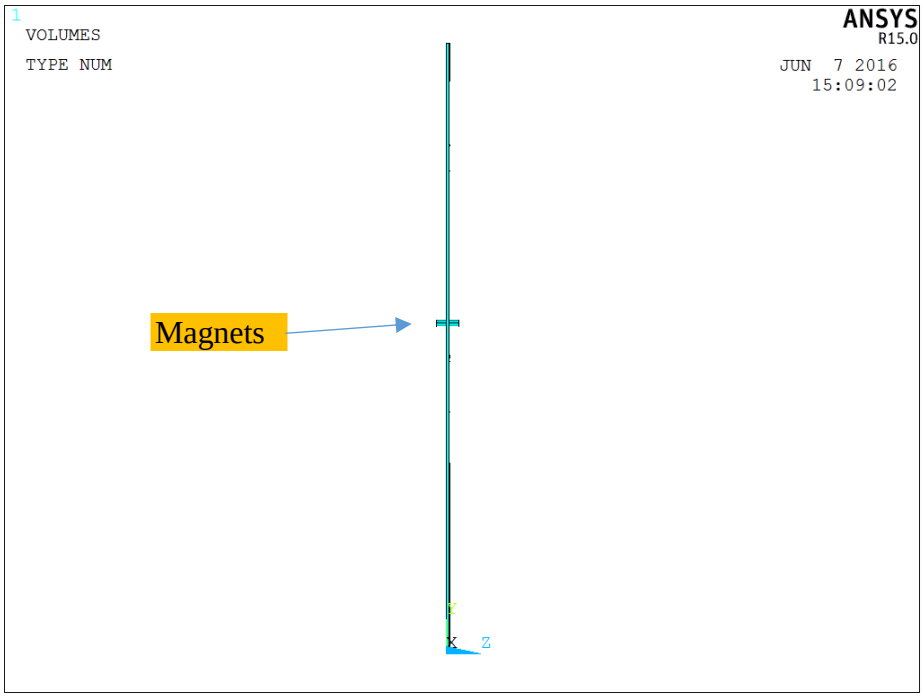

(c)

Figure 1. (a) Finite element model in front view (b) Three dimensional finite element model (c) Three dimensional finite element model in side view

The simulation needs a coupled thermos-mechanical model for the laser-induced acoustic wave propagation. The element types of both laser hitting point and aluminum plate are tetrahedral 10 node SOLID187 structural element. The origin of the coordinates is located at the left-bottom of the plate. Before meshing the whole 3D model, different material properties are attributed to different part of the model. Very fine mesh near the heating source location is used for the computational accuracy.

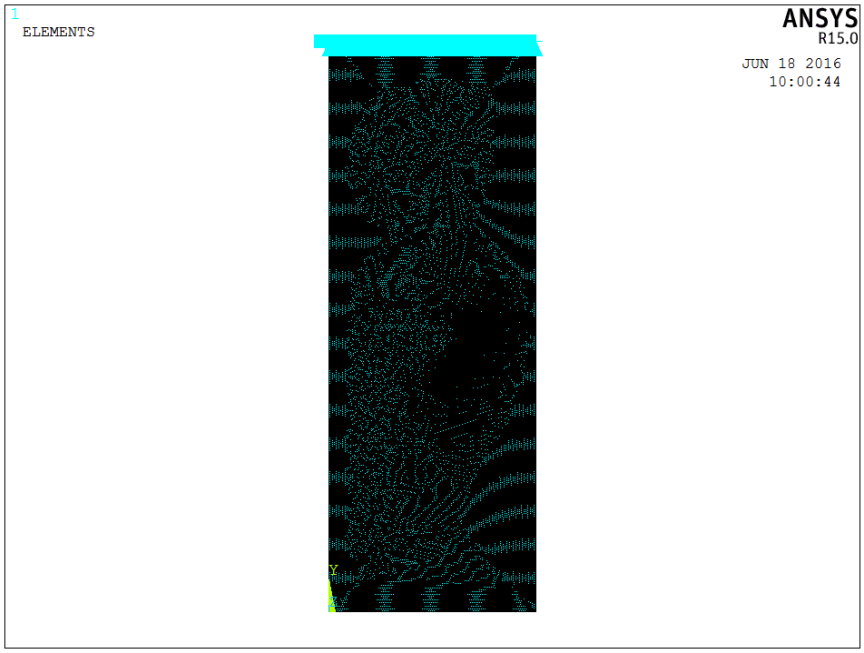

(a)

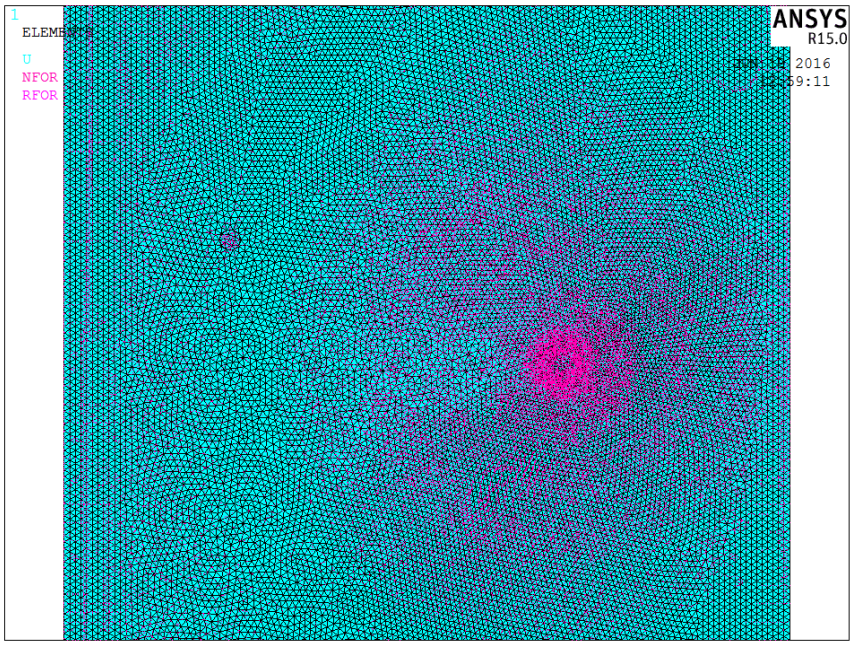

(b)

Figure 2. (a) The whole model after meshing (b) Meshed area of laser beam and meshed area of damage area

Since the laser-induced heating only affects a very small volume of materials and there is no need to perform the coupled thermos-mechanical analysis for the entire model, which is too expensive. The proposed study used a sub-model with coupled thermos-mechanical analysis and the global model for pure mechanical analysis to achieve the computational accuracy and efficiency. The proposed methodology needs to define two sets of material properties: the first one was attributed to laser beam shooting area which includes Young's modulus, Poisson ratio, density and thermal expansion coefficient. The second one was purely structural model which only been defined by Young's modulus, Poisson ratio, and density. The Young's modulus of the aluminum plate is 69×10^9 Pa, Poisson ratio is 0.33, density of aluminum is 2720kg/m^3, thermal expansion coefficient is 23.1×10^{-6}/k. Reference temperature is 273.15 K.

2.2 Laser induced loading function

The rigorous simulation for laser-induced acoustic wave propagation needs a coupled opto-thermo-mechanical analysis, which is very complex. This can be simplified for the damage detection problem as the laser speed is much faster than the thermal diffusion and wave propagation. A simplified loading function due to laser heating is proposed and the following hypothesis are used: (1) the heating profile follows the laser firing profile and the light speed is ignored; (2) the opto-thermal conversion efficiency is assumed to be a constant for the investigated metal. Similar assumptions have been used in other studies. It should be noted that the quantitative conversion efficiency of laser to heat flux is beyond the scope of this study and is not necessary if the final objective is the wave speed and time of flight for damage detection. As long as the material remains in the thermal-elastic region, the magnitude of the conversion factor only affects the local temperature peak value (and

the wave magnitude due to thermal expansion). The proposed study focuses on the phase information and the loading profile of the applied heat source function is set as a step function, which is:

$$\text{Temperature} = \begin{cases} 273.15K & 0\ ms < t < 0.1ms \\ 274.35\text{K} & 0.1ms < t < 0.6ms \\ 273.15K & 0.6ms < t < 1ms \end{cases}$$

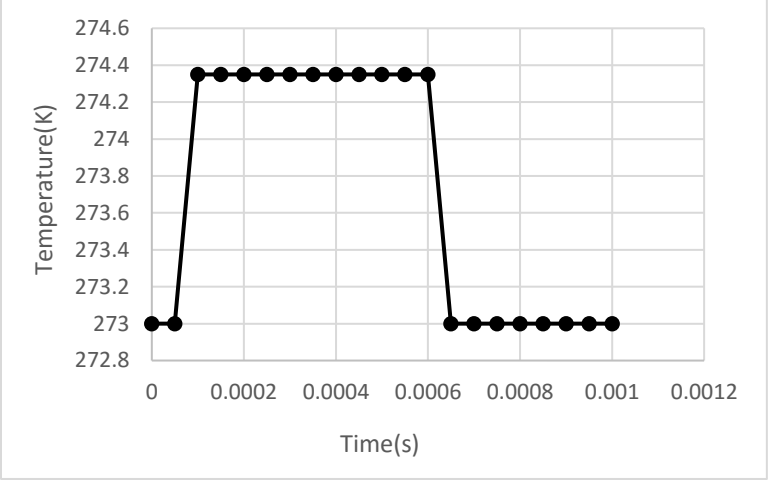

Figure 3. Temperature loading function

When the time is from 0ms to 0.1ms, the temperature is at reference temperature which was 273.15K. There was no loading applied on the specimen. Starting from 0.1ms, 274.35K is applied on the projection area of the laser beam and formed an impact loading. The loading temperature was estimated by referring the research which studied the relationship between applied time and temperature increment[24], this estimated temperature value may not influence the time history of the received signal only have an effect on magnitude of the specific values such as displacement, velocity and stress. This process lasted for 0.5ms until the time to 0.6ms, this temperature loading ended. In the rest time from

0.6ms to 1ms, there was no temperature loading on the specimen and its temperature returned to reference temperature which is 273.15K. For the boundary condition, following the condition of the experiment, the upper side of the specimen plate was fixed by x and y direction. It should be noted that the temperature after the laser firing may return to reference temperature in a longer time and proposed temperature profile is a highly simplified function which assumes that rapid thermal diffusion. This simplification will not affect the damage detection much (shown in Chapter 3) as only the first timing window of the received signal is critical. The post-firing temperature history does not contribute much to the received signal.

2.3 Simulation results and discussion

Several simulations have been done using the developed FEM methodology. The focus is on the time of arrival and wave speed in the testing article. The results are shown below.

2.3.1 Simulation results along vertical path

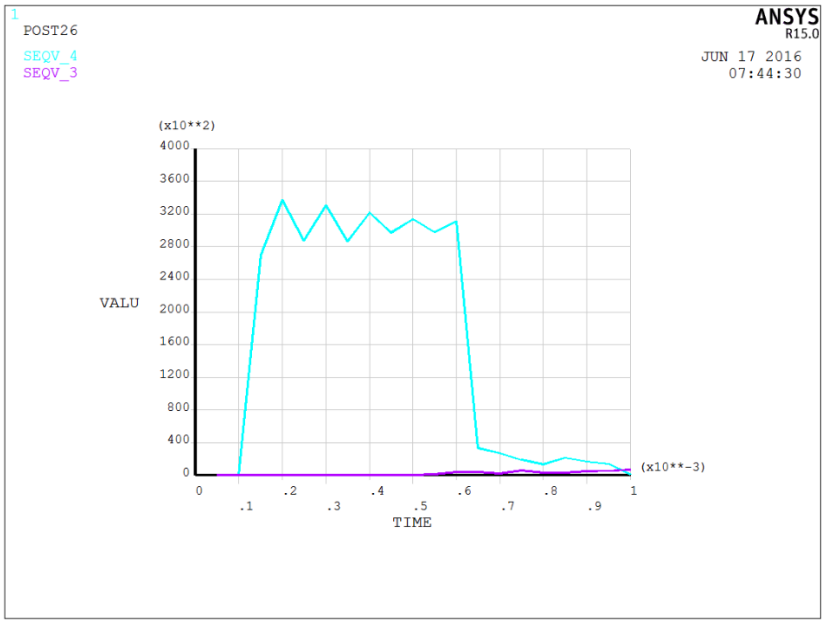

Figure 4. Vertival path test--Time history profile of von Mises stress in simulation

The figure above shows the time history for the von Mises stress of the emission point and receiving point. The blue line represents the laser signal which starts from 0.1ms to 0.6ms, the laser pulse duration is 0.5ms. The purple line represents the receiving signal from the sensor, the signal is not very obvious due to the temperature magnitude is small. The initial point of the received signal can be identified in this graph. When the time reached to 0.5ms, the signal starts going up. The temperature load is applied at 0.1ms, so the time of arrival can be obtained by computing the difference between these two time values which is 0.4ms.

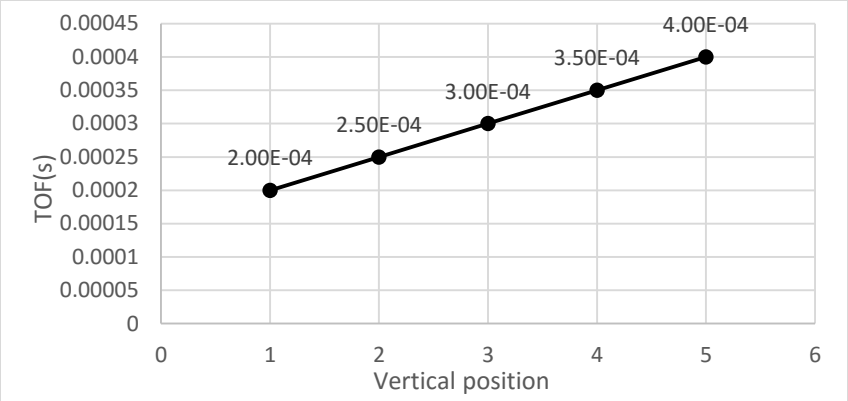

Figure 5. Time of arrival when laser beam vertically move in simulation

Other simulations have been done along the vertical path. The distance between the laser hitting point and the sensor location increases. Thus, the time of arrival is increasing as the distance increases (Fig. 5). It is linearly increasing as shown in figure 6. The time of arrival is 0.2ms when the laser hitting point located at point 1 which is the nearest point from sensor location.

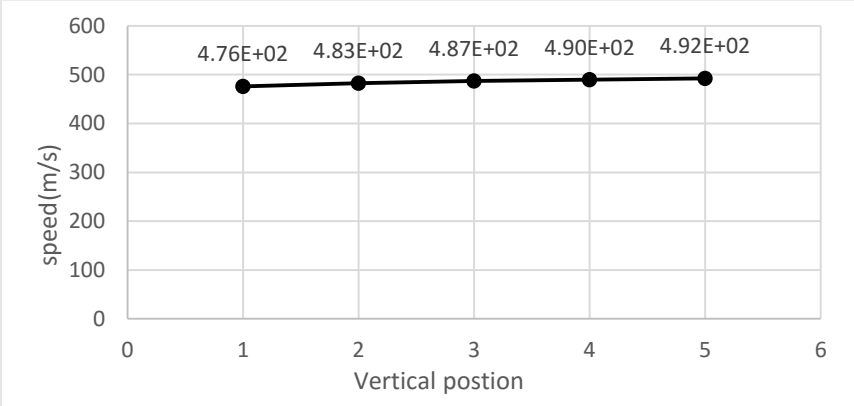

Figure 6. Wave speed when laser beam vertically move in simulation

In figure 6, the speed of the stress wave propagated in the aluminum plate keeps constant, and the value of speed is around 500m/s. It should be noted that this value is

relatively small and that is because a mass point is set along the path, which decreases the wave speed. The wave speed does not change, much with the change of distance.

2.3.2 Simulation along the horizontal path

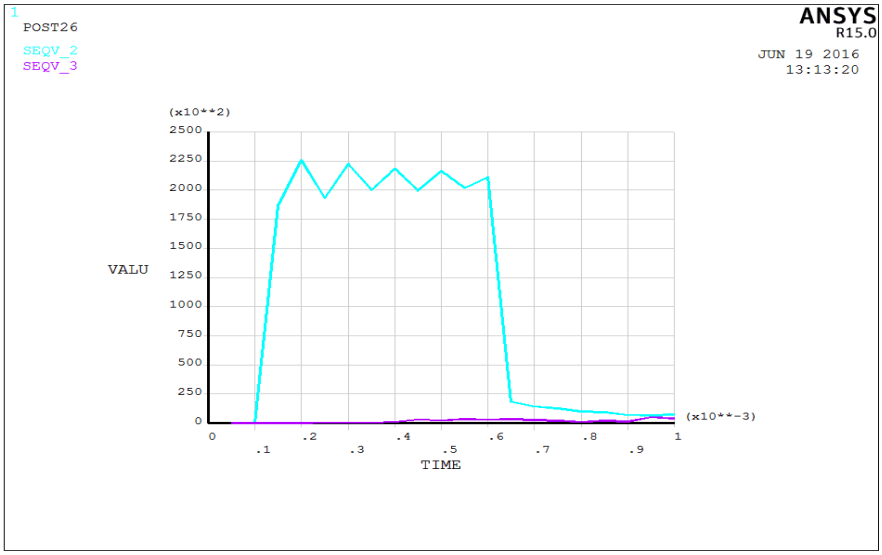

Figure 7. Horizontal path test--Time history profile of von Mises stress in simulation

The time history of von Mises stress was also used to analyze the time of arrival along the horizontal path (Fig. 7). Blue curve represents the time history of stress in laser hitting point. From the figure above, the temperature was applied from 0.1ms to 0.6ms, stress also increases from 0.1ms, and ended at 0.6ms. Purple curve is the time history of stress in sensor location. The line starts going up at 0.35ms, this means sensor received stress wave at 0.35ms. Got the initial time of the stress wave, the time of arrival could be simply calculated. The time difference is 0.25ms, which is also the time of arrival.

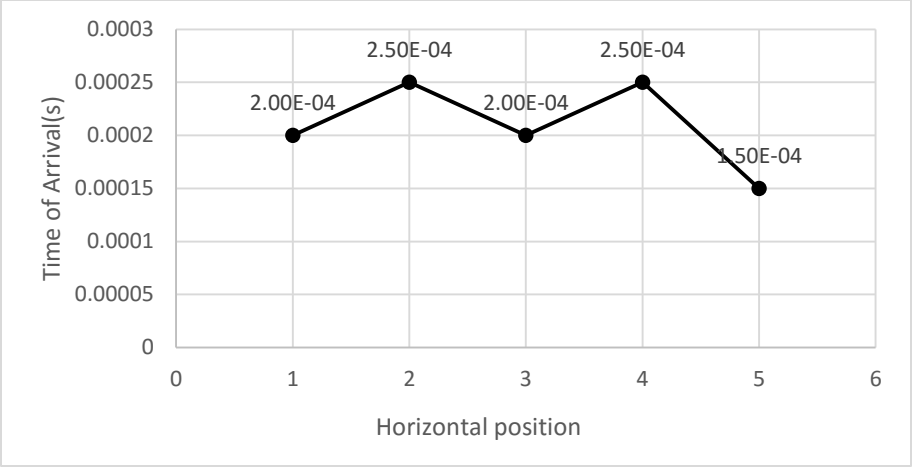

Figure 8. Time of arrival when laser beam horizontally move in simulation

When doing the horizontal move in the simulation, the damage which is the magnet in the test is attached on the surface of specimen. The location and dimension of the magnet are exactly the same with real magnets used in the test. Magnet led to the longer duration of the time of arrival due to the increases local mass. When moving the laser beam to the right point in the horizontal direction, the magnet influence on the stress wave propagation should decrease and the path is moving away from the magnet location. It is expected that there is a region within which the wave speed is lower than those in the virgin materials. This is shown in Figs. 8-9. In Fig. 8, it is observed that a reduction of TOF at point 5, which is far away from the magnet.

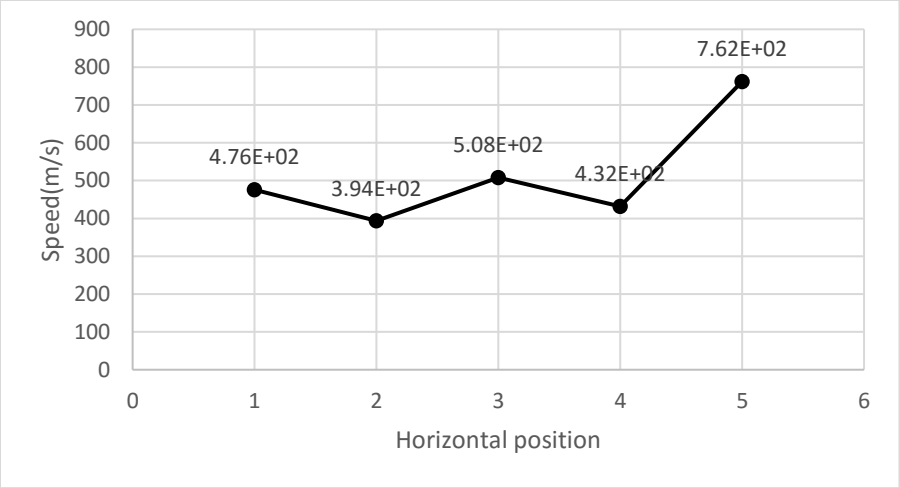

Figure 9. Speed when laser beam horizontally move in simulation

The result shown in Fig. 9 indicates that the speed increases when the path of the propagation wave getting far away from the local mass. It appears that there is a region where the magnet reduces the TOF estimation and the effect decreases when the path is beyond this region.

2.3.3 Effect of number of magnets simulation results

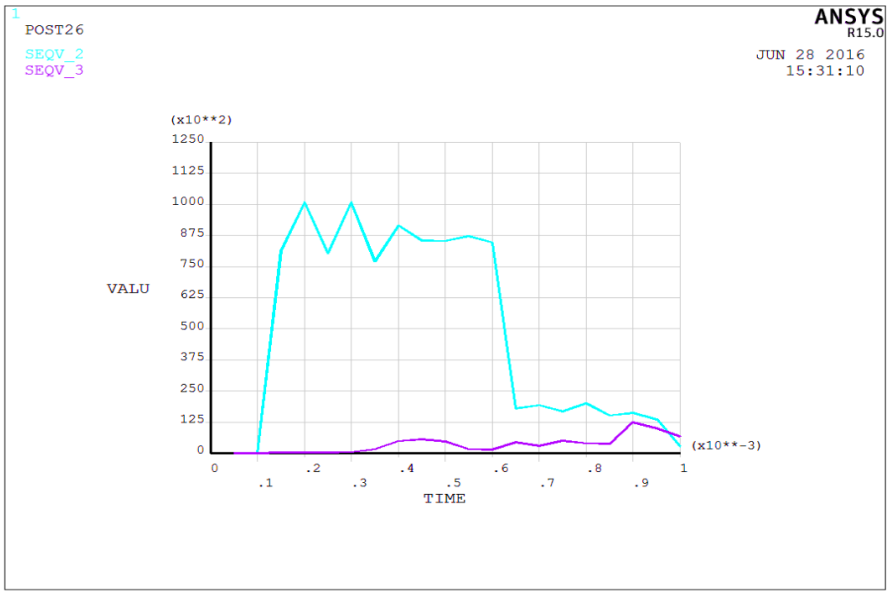

Figure 10. Effect of number of magnets test--Time history profile of von Mises stress in simulation

Time history profile of simulation with different number of magnets is shown in figure 10. The blue line indicates the stress change with time caused by laser beam signal and the purple line represents the stress change received by sensor. Purple line starts to going up at the time of 0.3ms when the temperature load applied at the time of 0.1ms. Therefore, the time of arrival in this case is the time difference between these two time values which is 0.2ms.

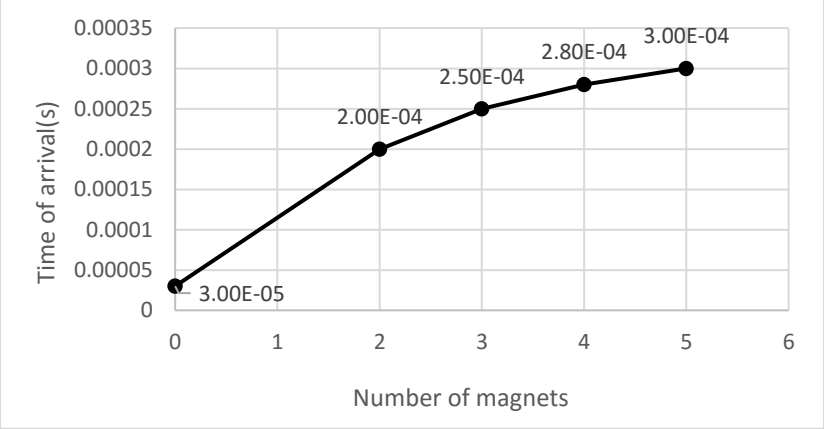

Figure 11. Time of arrival when adding the number of magnets in simulation

When the number of magnet is 0, time of arrival is the minimum due to wave propagation medium is homogeneous aluminum material. The thickness and density of the medium do not change during the wave propagating in the path. When adding magnets, the local mass will be increased and this change will led to the increase of the time of arrival. By adding the magnet one by one each test, time of arrival gradually increases. Therefore,

the conclusion could be obtained that adding more number of magnets, the time of arrival will become longer. The trend is not linear and is shown in Fig. 11.

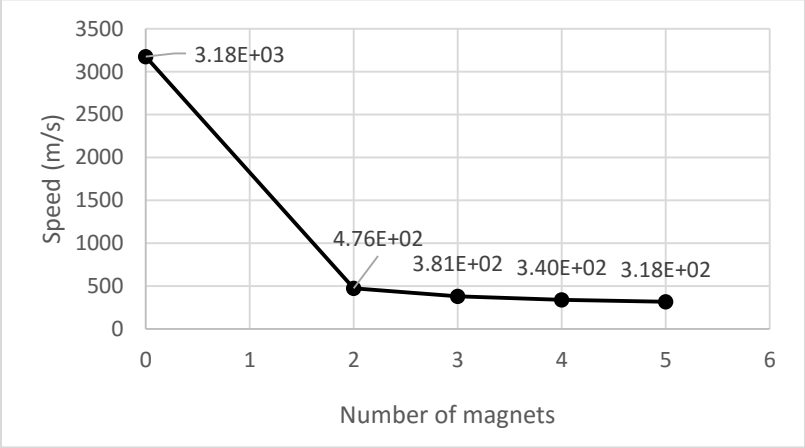

Figure 12. Speed when adding the number of magnets in simulation

In Fig. 12, the speed reaches maximum due to there is no magnet in the propagation path, after adding two magnets, speed of the wave suddenly reduces. The reason of this phenomenon is adding two magnets at one time dramatically change the properties of the wave propagation medium. Thus, wave speed decreases significantly. With the number of magnets gradually increasing, the wave speed gradually reduces.

A short summary can be achieved from the above simulation results.

- The numerical simulation shows that the wave speed is almost constant if the wave propagation pass have no mass change. The speed is about 500m/s with two small magnets;

- The wave speed will increase when the ray path is far away from the mass point. The speed without added magnet is about 3200m/s in the current laser firing conditions for the first received wave window;
- The increase of magnets numbers (e.g., mass) will decrease the wave speed. The relationship is not linear and the sensitivity is high for small increases of local masses.

The numerical simulation clearly indicates that the laser induced acoustic wave using the current setup is able to identify the local property changes. Most structural damage can be simplified as the local mass change (e.g., cracks and voids) or stiffness change. The numerical simulation indicates that these changes can be detected using the TOF changes. Experimental testing discussed below will further support this statement.

Chapter 3

EXPERIMENTAL INVESTIGATION OF OPTOACOUSTIC WAVE PROPAGATION

3.1 Overview of the laser-induced optoacoustic wave propagation testing

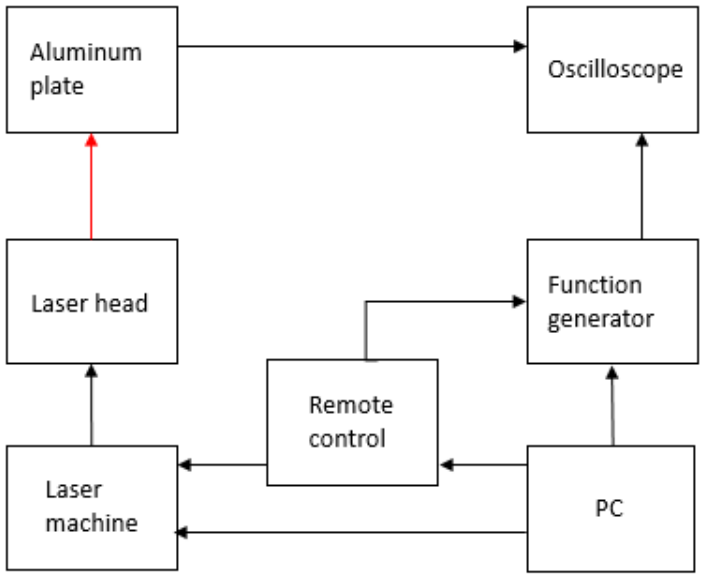

Figure 13. Schematic diagram of experimental investigation of wave propagation

In-house experimental testing is performed to validate the numerical simulation results in Chapter 2 and to demonstrate the feasibility of the proposed laser-induced optoacoustic wave propagation methodology for damage detections. An overall schematic illustration of the experimental testing methodology is shown in Fig. 16 for its major components.

Computer controls the function generator to simulate the square wave to the laser control machine. The laser will be fired to shoot the specimen plate. There are two sensors attached in the specimen to receive the stress wave. An oscilloscope will show both the

received signals and the laser excitation signal which is synchronized from the function generator. All data will be transferred back to the computer for further analysis. The entire automation is programmed using Labview.

In the testing, the pulse duration is set to 200ns and the pulse repetition rate is 100 kHz. The frequency of the square wave which generated by the function generator is 1000Hz.The duty cycle is 50%. Therefore, there are 50000 laser pulses fired in one square wave. The largest frequency of the square wave is 1000Hz which means the smallest square wave duration is 1ms. In the current setup, if the frequency is larger than 1000Hz, signals would not be received by the sensor and there are no signals showing on the oscilloscope. This is probably due that the laser energy is too small for very high frequency firing. The order of magnitude of time difference got from the testing can reach 0.0001ms. For every point of the surface in the test specimen, a fast firing of the laser beam forming a short period of thermal excitation, which will make a thermal expansion of the point under laser beam, this expansion results in an in-plane stress wave through the whole test specimen, when the stress wave propagate to the sensor, it will receive the wave and obtain the displacement and time relationship, from this relationship, the time of arrival will be obtained.

3.2 Experiment setup

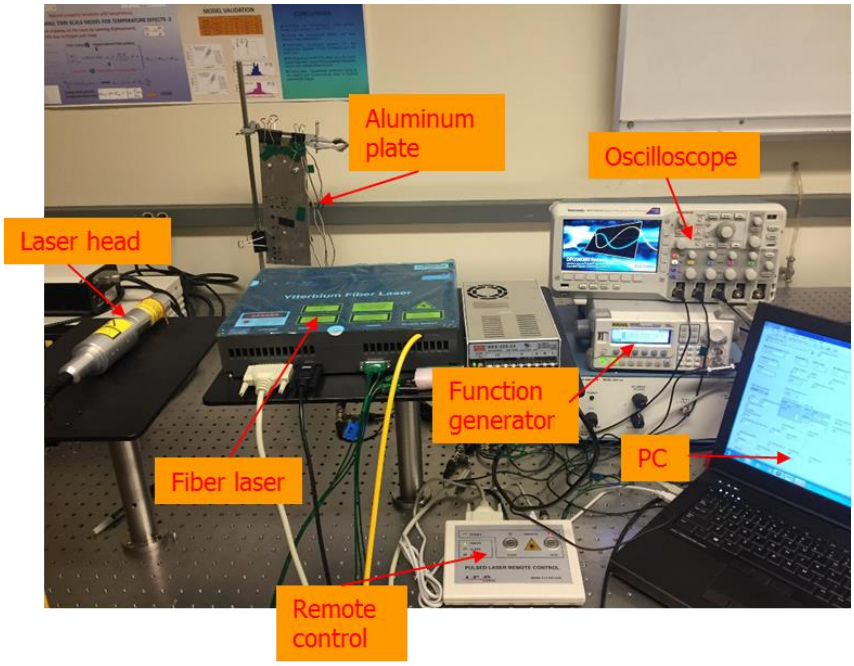

Figure 14. Setup of the laser scanning testing

There are seven parts in this experiment. An aluminum plate which is the specimen with attached magnets as the damage. A Tektronix DPO 2024B oscilloscope is used to collect the signals received from the sensors and RIGOL DG1022 function generators which is controlled by computer. The computer also controlled the function generator to generate a square wave which used by the laser controller to synchronize the laser firing. Laser beam is generated by an IPG YLPM-1-4X200-20-20 Ytterbium Fiber Laser machine. This laser machine consists of a laser head, a controller, an IPG YLP-RC-USB remote control box, and a computer control panel. Computer control panel is used to set the laser power, to change pulse repetition rate, to turn on/off the emission, and to monitor the status of the laser. Controller provides power to the laser head and get connection to the computer. Remote control box turn on and off the laser beam which emits from the laser head. Laser

head is used to launch the laser beam to the plate and show the location of the laser beam in the specimen with a secondary aiming red laser. The setup is shown in Fig. 15.

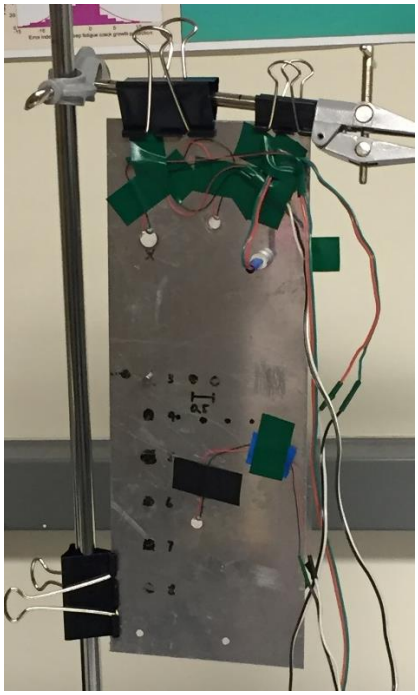

Figure 15. Configuration of the specimen

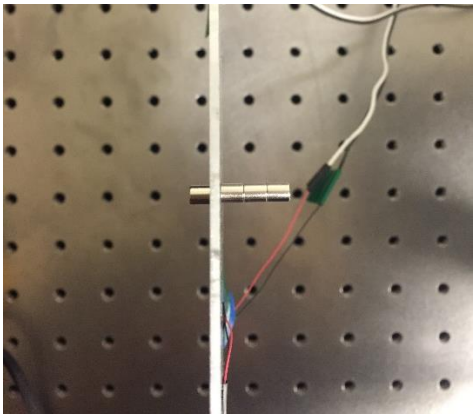

Figure 16. Location of the glued magnets

Specimen is an aluminum plate which is fixed at the upper end in a holder stands 0.5m away from the laser head. There are totally three sensors glued on the specimen, they have different thickness and different frequency range to receive signals, in the test, the sensors on the left and middle was used to receive the signal since the signal acquired from the sensor on the right is very weak and not clearly due to the sensor parameters, therefore, the signals received from left sensor were used to do analysis. And the sensor attached on the lower part of the specimen was not used in this experiment. There are two directions of scan tracks located on the lower part of the specimen, the black dots which indicates the locations of the laser beam (from point 4 to point 8). In the horizontal direction, laser beam starts from point 4 to the right 4 positions. Instead of make a crack in the specimen, the magnets are used to represent the damage in the test. Therefore, when did the test, by adding the number of magnets (Fig.16) the change of the wave propagation speed could be obtained.

3.3 Signal processing and system delay compensation

The signal processing is also an important part of the test especially for the proposed methodology. The used low power MOPA laser source generates a low amplitude acoustic wave and the signal to noise ratio is low. Raw data were collected from the oscilloscope, which has been filtered by the internal low pass filter. The frequency of the low pass filter is 290kHz since the frequency of the laser is set up as 100kHz. After getting the raw data for both laser signal and sensor received signal, these data were applied by the Butterworth band pass filter as the Laser-generated acoustic wave is a wide-band signal. The upper and lower band of the band pass filter are 500Hz to 1500Hz due to the frequency of excited signal is 1000Hz. For the received signal, 80kHz and 120kHz are the upper band

and lower band since the laser pulse repetition rate is 100kHz. Sampling frequency is 62.5MHz and the power of laser was set to be 90.6% of the full power.

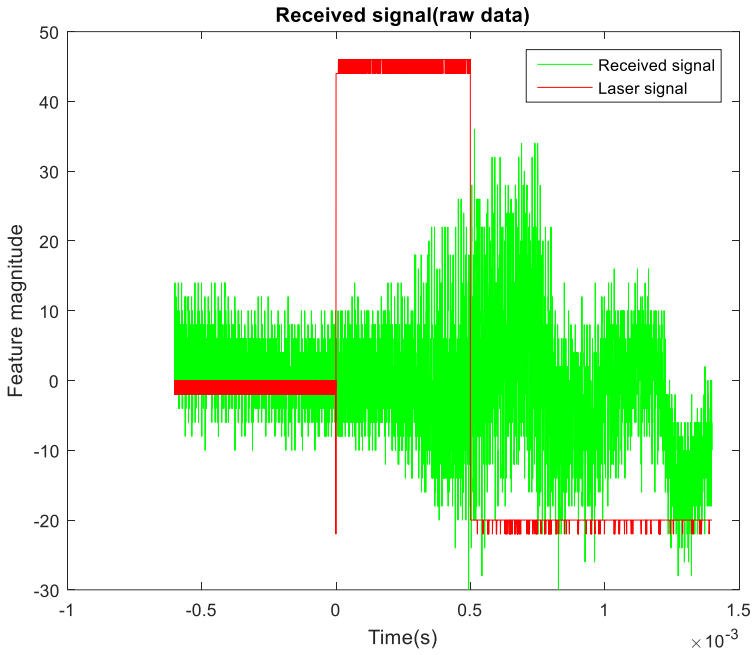

Figure 17. Raw data collected from oscilloscope

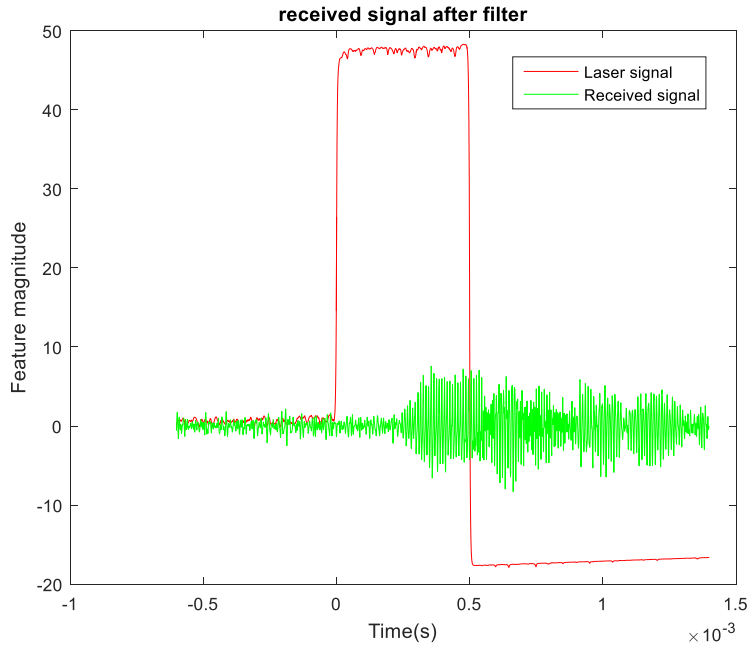

Figure 18. Filtered signal with band pass filter

From the figures above, laser signal which is the red signal could be clearly recognized and the initial point of the signal rising can be determined. The green lines represents the signal received by the piezo sensor and contains large noises. Therefore, another method called Hilbert-Huang transformation was employed to this filtered received signal[25]. This method could decompose the nonstationary signal into intrinsic mode functions.

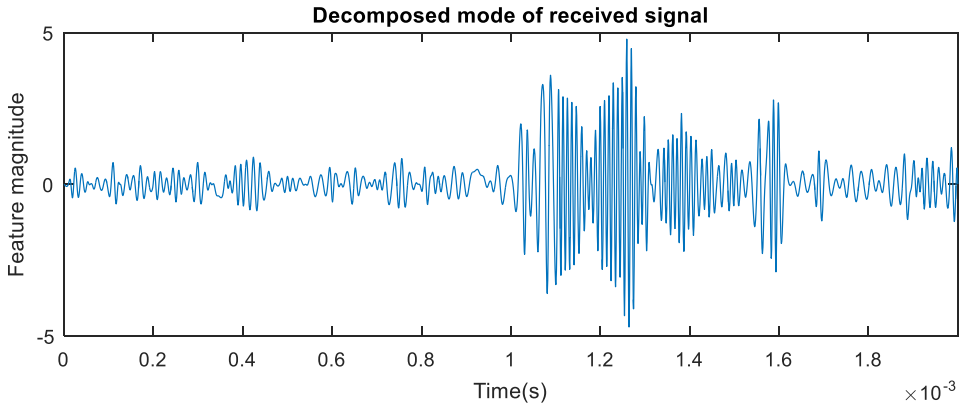

Figure 19. Decomposed signal

In the figure above, the initial point of the received signal is easy to identify, it locates at around 0.9ms.

Another important processing the compensation of the controller delay. Laser beam was excited by the electrical signal of the function generator. When the commands are sent through the computer software to function generator and laser controller, there was a time delay between the time of sending commands and the time of laser firing Thus, a calibration test was applied to get the value of this time delay. The laser hitting point is very close to the sensor and the TOF for the wave propagation is ignored. This test is repeated 3 times

and the average value of time delay can be quantified. The time delay caused by the system is estimated to be 0.786ms, this value should be subtracted from the time of arrival obtained from normal testing.

3.3.1 Experimental parameter setup

3.3.3.1 Testing parameter determination

Pulse duration, pulse repetition rate, and excitation pulse duration of the laser signal were changed to do the experiment in order to determine the best combination of the parameters to generate acoustic waves in the aluminum plate. 8 pulse durations are chosen, i.e., 4ns, 8ns, 14ns, 20ns, 30ns, 50ns, 100ns and 200ns. 4 sets of pulse repetition rate are chosen to do analysis, which are 20kHz, 100kHz, 150kHz and 200kHz. Table 1 shows qualitative justification to the received signal at different pulse durations and different pulse repetition rates. The justification is based on the signals shown below. The screen shots for the oscilloscope are shown for the laser signal and signals from the two receiving sensors. It should be noted that these are the representative signal patterns as indicated in Table 1. For small laser duration, the received signal is too weak to be identified. This is due to the used low power MOPA laser and indicates a certain energy level must be reached to generate sufficient acoustic wave to be detected. For high pulse repetition rate, the signal can be received but the signal to noise ratio is very low. This is due to the certain resonance frequency of the piezo sensors. From the Table 1, the clearest signal could be obtained when pulse repetition rate were 20 kHz and 100 kHz. 200ns pulse duration and 100 kHz pulse repetition rate were the best combination to do the test.

Table 1 Signals in different pulse duration and pulse repetition rate

Pulse duration / Pulse repetition rate	4ns	8ns	14ns	20ns	30ns	50ns	100ns	200ns
20kHz	○	○	◐	◐	◐	◐	●	●
100kHz	◐	◐	●	●	●	●	●	●
150kHz	◐	◐	●	●	●	●	●	●
200kHz	●	●	●	●	●	●	●	●

Note:		
	○	There is no signal received.
	◐	There is signal received but not very clear.
	●	There is signal received.
	●	There is signal received and it is the clearest signal.

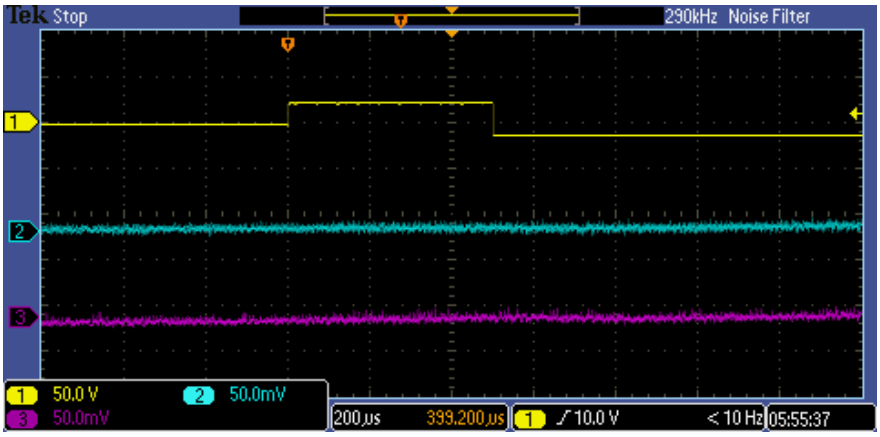

(a)

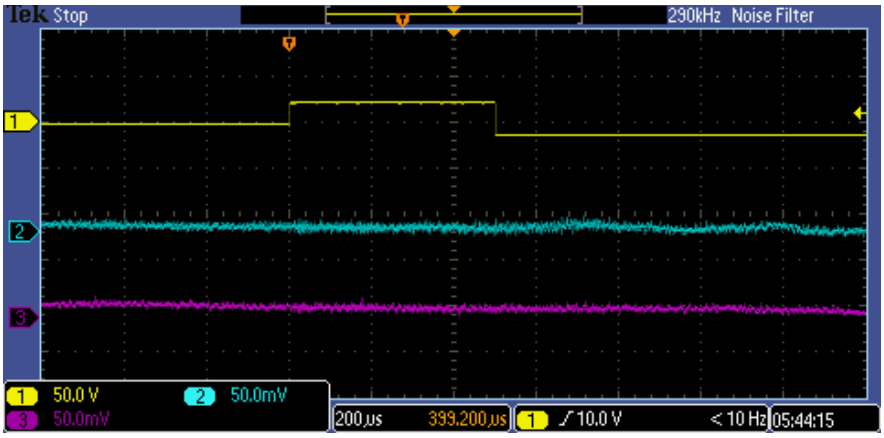

(b)

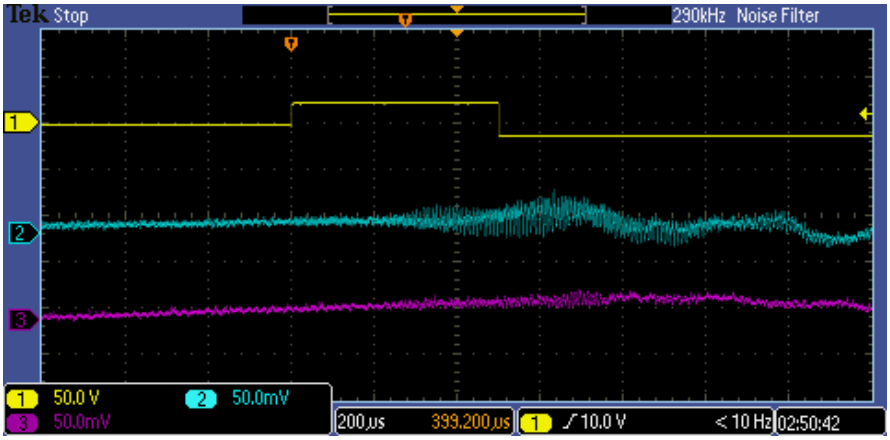

(c)

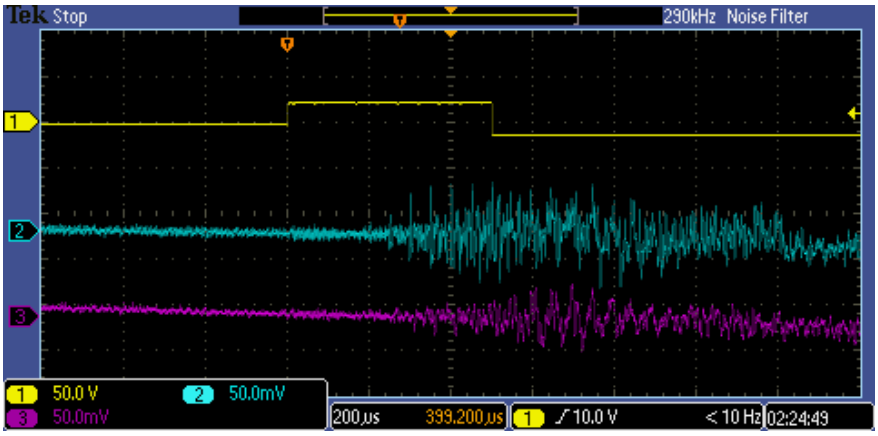

(d)

Figure 20. (a) There is no signal received from the sensor (b) There is signal received but not very clear (c) There is signal received (d) There is signal received and it is the clearest signal

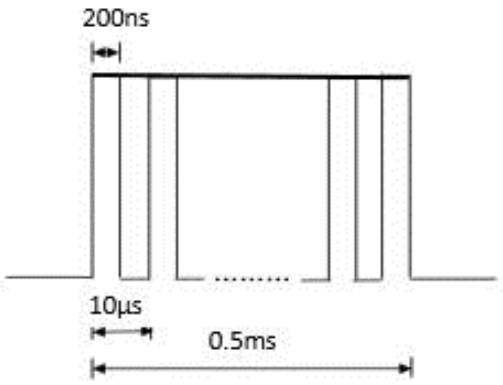

Figure 21. Pulse parameter setup

Due to the minimum limitation of the excitation pulse duration is 1s and duty cycle is 50%, 0.5s is the minimum excitation pulse duration applied to this test. Figure 25 shows the pulse parameter in the experiment. Pulse duration was 200ns, pulse repetition rate is 100 kHz and excitation pulse duration is 0.5s, which means there were 50000 laser pulses were shot to the specimen when the function generator excited once.

3.4 Convergence study

Due to the large noise associated with the experimental testing, repeated testing and averaging needs to be used to reduce the error. There is always a trade-off between the measurement accuracy and efficiency. Thus, a convergence study is employed to find the best number of repeating tests to balance the measurement accuracy and testing time.

Convergence of both time of arrival and speed are analyzed by fixing the laser hitting point to point 1 and adding two magnets on the specimen. All the parameters are the same as the previous setup. The testing is continuously repeated for 32 times. The averaged values are plotted with respect to the number of repetitions in Figs. 41-42. It appears that the results converge after about 5~10 repetitions.

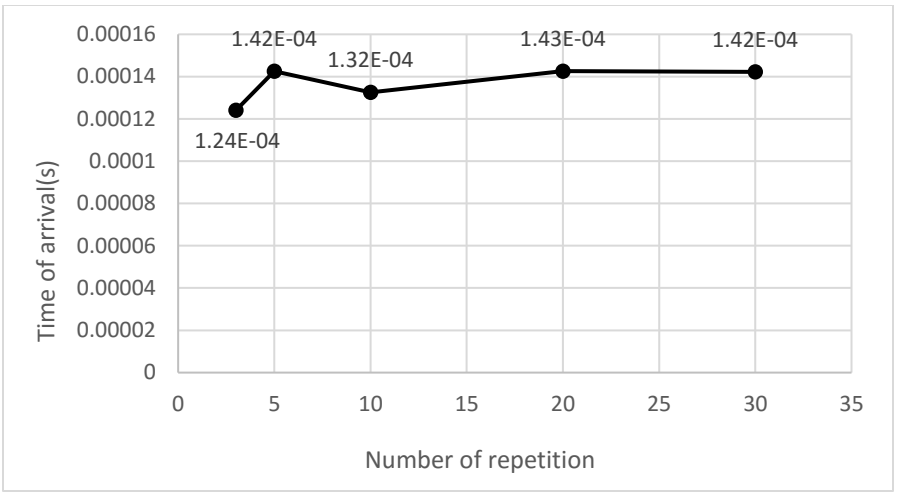

(a)

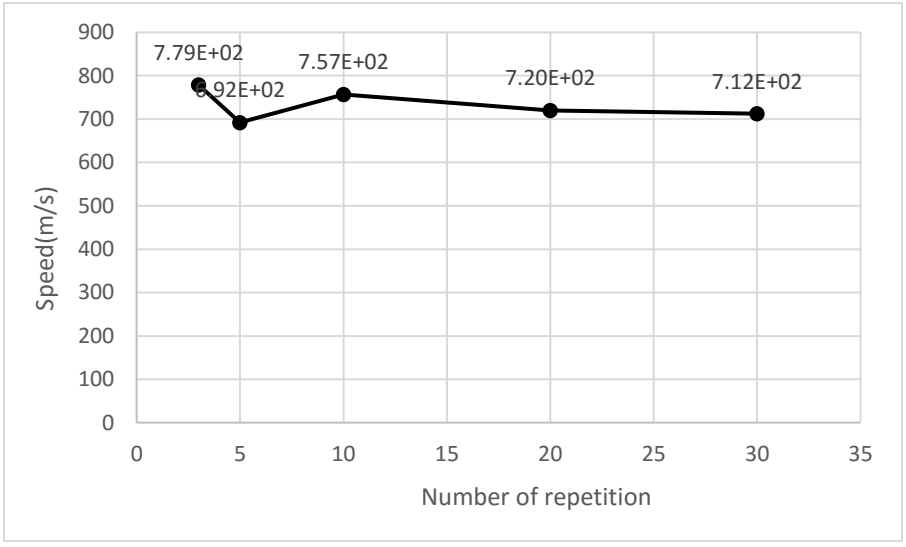

(b)

Figure 22. Convergence study for (a) time of arrival (b) wave speed

From the two figures above, time of arrival in figure 41 convergent when the number of repetition reaches 20 and 30, the time of arrival becomes a constant which is 0.142ms.

Wave speed also convergent when the times of test repeat many times, the convergence value of the speed is 712 m/s.

3.5 Experiment results

Similar experimental testing with those shown in the numerical simulation have been performed. The first part is the change of the vertical position of the laser hitting point. The second one is the change of laser shooting location horizontally. The third one is the testing with different number of magnets.

3.5.1 Vertical path test

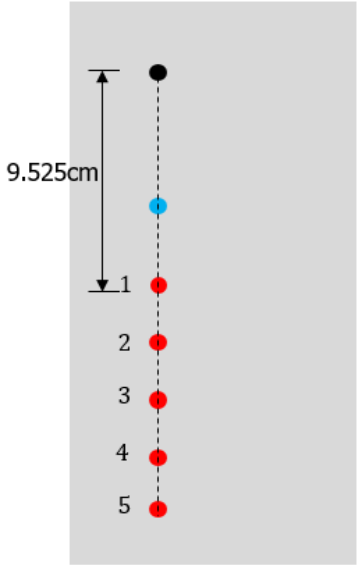

Figure 23. Configuration of the vertical path test

In this test, both the sensors and the magnets were fixed, the location of the laser hitting point on the aluminum plate starts from the point 1 to point 5. The distance between sensor 1 and laser beam position1 is 0.09525m. The distance between adjacent points is 0.0254m. The magnet locates in the middle of the sensor and laser hitting point as the blue point shown in the figure 19. The number of magnets is two and is fixed during the testing.

At the beginning of the test, the laser hitting point is located on point1 as shown in figure 23. When laser beam moved from point1 to point 5, the distance between the laser beam and the sensor increases. The time of arrival also increases with the distance increments. The speeds of the stress wave are around 500m/s, which has the similar speed value with simulation results. Due to the same medium exist in the path of the wave propagation, speed of the stress wave should keep constant no matter where the laser hitting point is locating. In the experimental testing, some variations can be observed due to the measurements errors. Detailed results are shown in Table 2 and Figs. 24-25.

Table 2. Time of arrival and speed of received signals in vertical move

vertical position	TOF(s)	Speed(m/s)
1	1.87E-04	5.21E+02
2	1.69E-04	5.84E+02
3	2.35E-04	6.03E+02
4	2.41E-04	5.52E+02
5	2.03E-04	6.28E+02

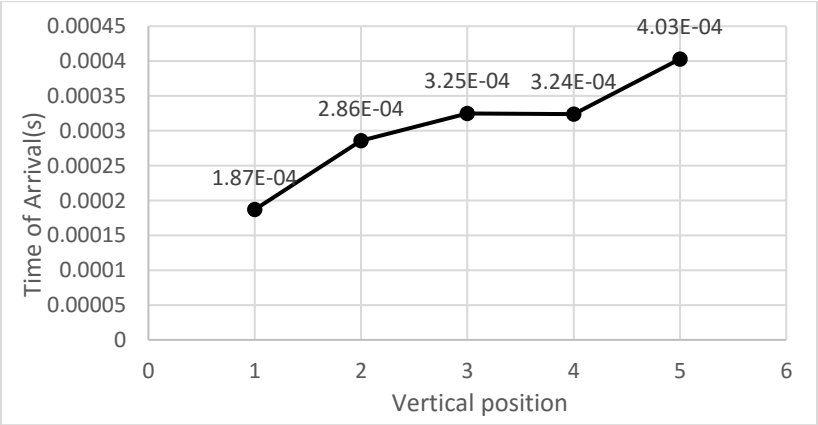

(a)

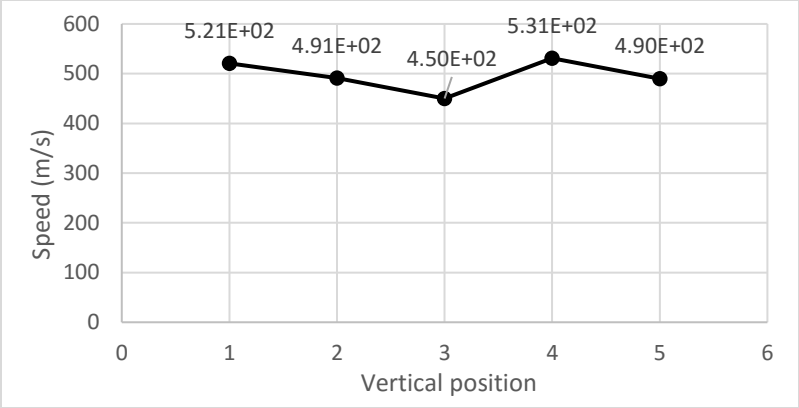

(b)

Figure 24. (a)Time of arrival (b) wave speed of received signals in vertical move

3.5.2 Horizontal paths test

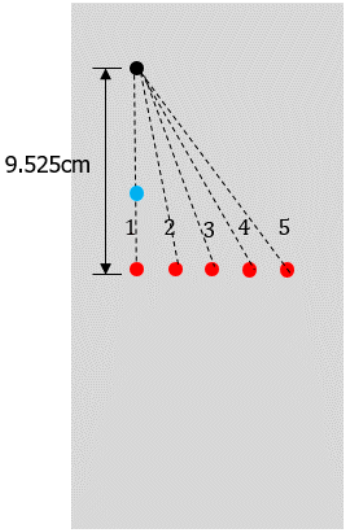

Figure 25. Configuration of the horizontal paths test

Figure 20 shows the path of the laser beam projection area in the horizontal direction. Laser beam point1 was 0.09525m away from the left piezo sensor, this point is the same point in the vertical path test. During the testing, the laser beam hitting point from

the left (point1) to the right (point5), which were the red points in the figure 20. The spacing of the adjacent points was 0.0127m. The location and number of the magnets was fixed, which was 2 magnets in the middle of the sensor and laser beam projection area.

Table 3. Time of arrival and speed of received signals in horizontal move

horizontal position	TOF(s)	Speed(m/s)
1	1.87E-04	5.21E+02
2	1.69E-04	5.84E+02
3	2.35E-04	6.03E+02
4	2.41E-04	5.52E+02
5	2.03E-04	6.28E+02

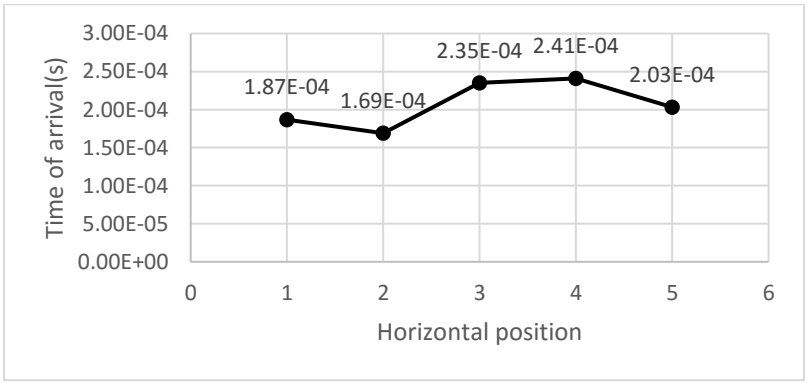

(a)

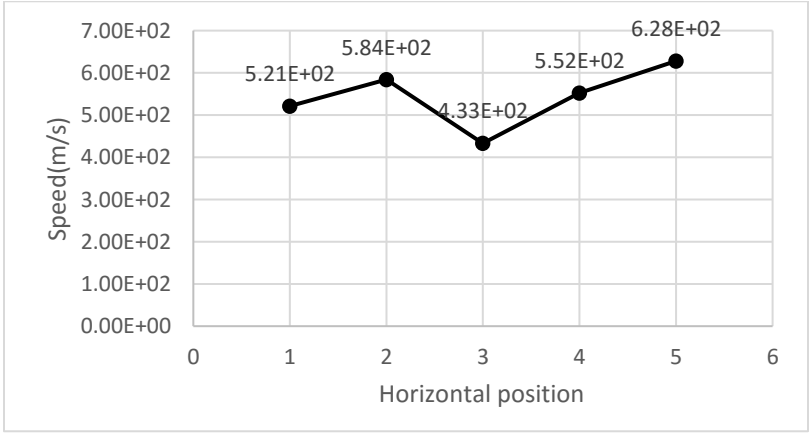

(b)

Figure 26. (a)Time of arrival (b) speed of received signals in horizontal move

In the figures above, the curve of stress wave speed increases according to the horizontal position of the laser beam. There is a magnet located at the wave propagation path between point 1 and sensor and the magnet will affect the propagation speed. From the figure 32, when laser locating at the point 1 which is the nearest point from the sensor, the speed is the smallest due to the influence of the magnet.

3.5.3 Testing with different number of magnets

The magnets in the test were treated as the damage in the specimen. By adding the number of the magnets, the speed of the in-plane stress wave reduces as expected. The laser hitting point is point 1. The results are shown in Table 4 and Figs. 28-29.

Table 4. Time of arrival and speed of received signals with increasing magnets

Magnets	TOF(s)	Speed(m/s)
0	4.92E-05	2.10E+03
1	1.87E-04	5.21E+02
2	2.40E-04	4.07E+02
3	3.02E-04	3.18E+02
4	4.59E-04	2.08E+02

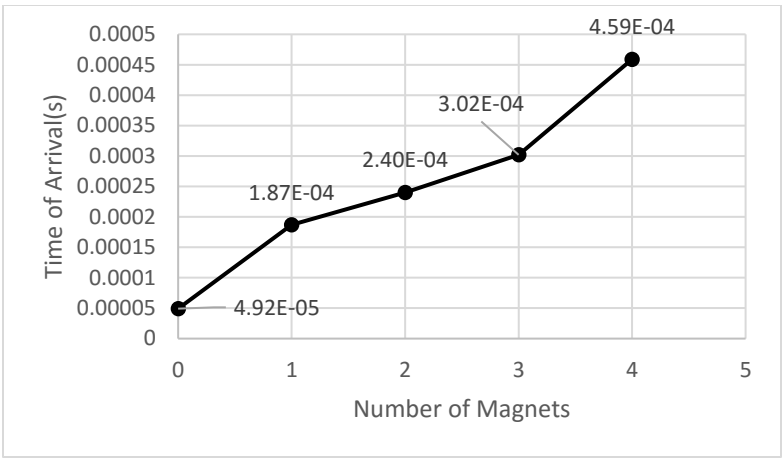

(a)

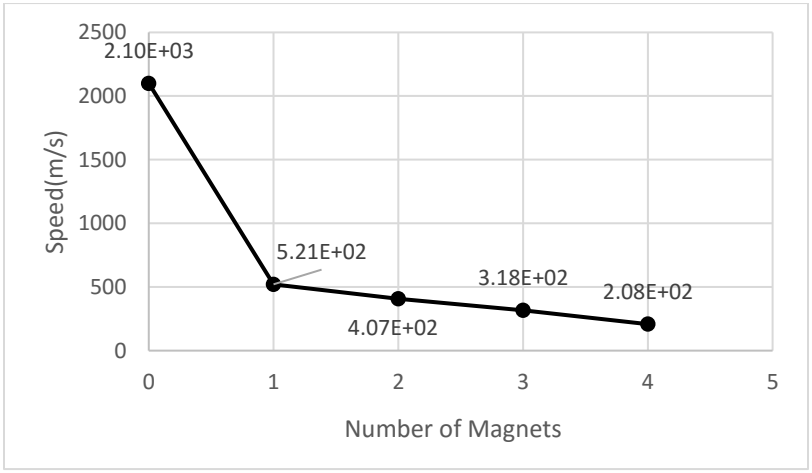

(b)

Figure 27. (a)Time of arrival (b) wave speed of received signals with increasing magnets

In the figures, x-axis of 0 means there is no magnet locating in the path of the wave propagation. Thus, the time of arrival is the smallest due to there is no added mass in specimen and the medium of the stress wave propagation is homogeneous. When there is no magnet attached in the specimen, the speed of the stress wave reaches 2100m/s. After adding the magnets to the path, the speed of the stress wave suddenly drop to 521m/s. As

the number of magnets increases, the speed of the stress wave reduces to about 200m/s with 4 magnets.

3.6 Comparison between experimental observation and simulation results

In the Chapter 2, the results of time of arrival and wave speed are obtained and analyzed using FEM. This section compares the experimental measurements with the numerical simulations for three groups of testing.

The experimental observations and simulations results are shown in Figs. 28. A satisfactory agreement between experimental data and simulations results is observed. The wave speed is almost constant with respect to the vertical path. Experimental data shows variations due to measurement errors.

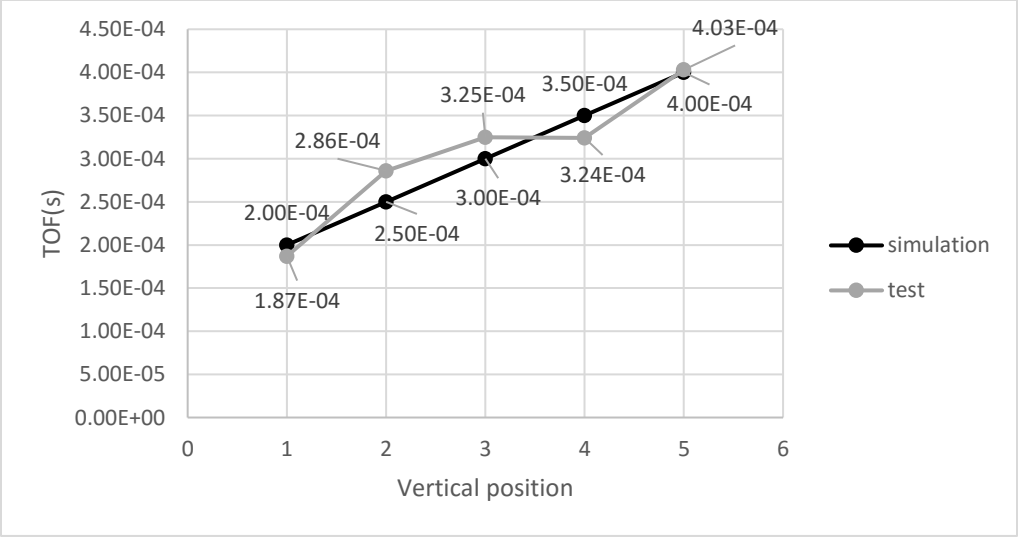

(a)

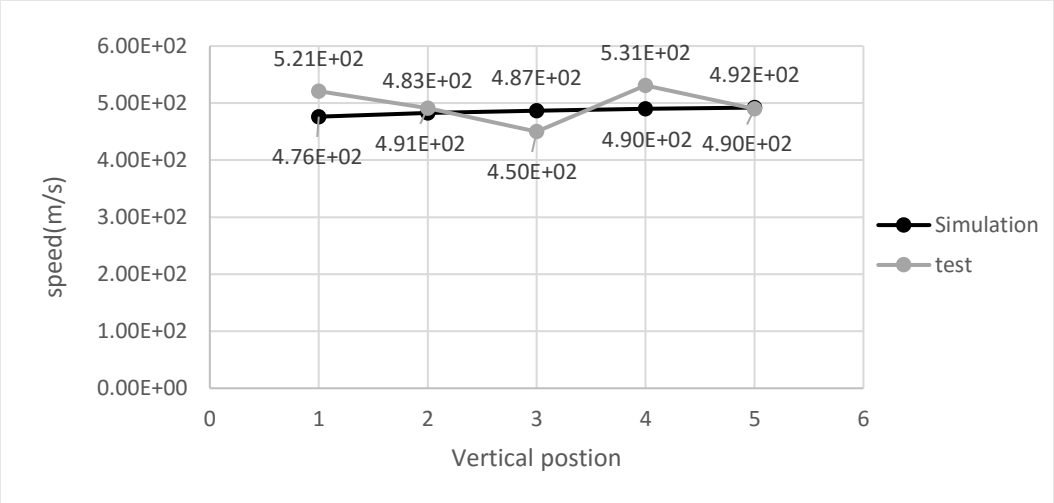

(b)

Figure 28. Test 1 results comparison of (a) time of arrival (b) wave speed

Similar comparison is performed for the horizontal tests and comparison is shown in Figs. 29. The agreement is not as good as the vertical path one, but the general trend is similar. The wave speed increases as the ray path is getting away from the mass. Both simulation and experimental results shows variations and this indicates that the TOF using the first arising time window may contain multiple wave modes. Future study is required to investigate this behavior.

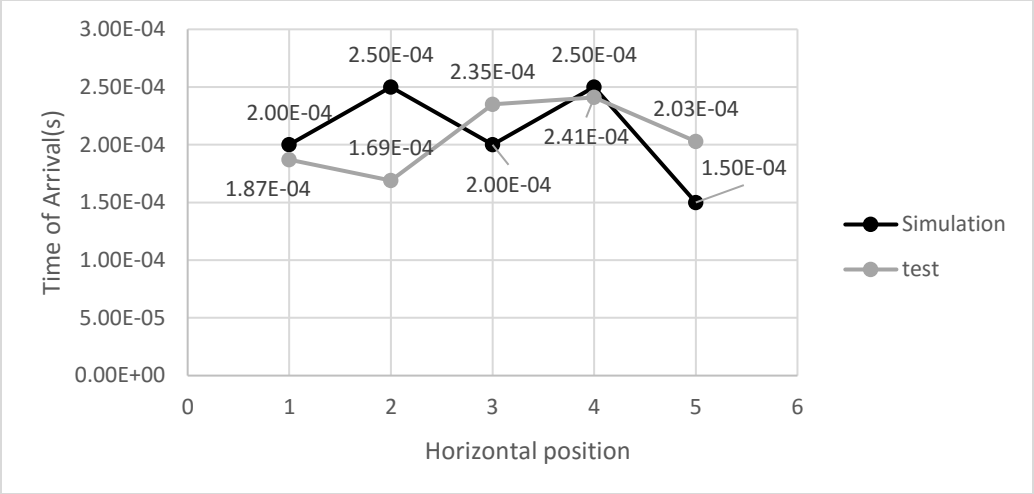

(a)

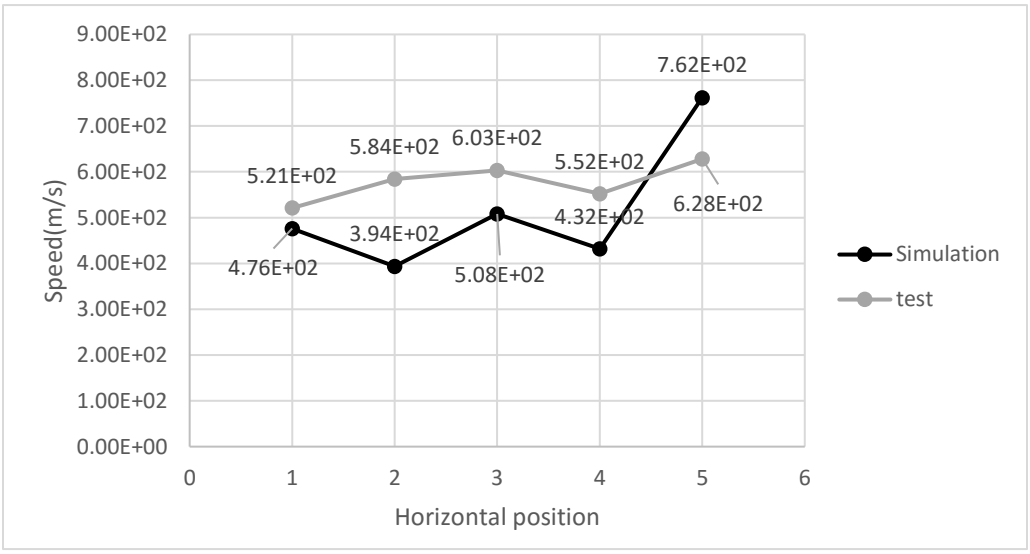

(b)

Figure 29. Test 2 results comparison of (a) time of arrival (b) wave speed

The final comparison is for the effect of different number of magnets and is shown in Fig. 30. Again, experimental observations strongly supports the numerical simulations. One large difference is observed for point 5 for the time of arrival. Further study is required.

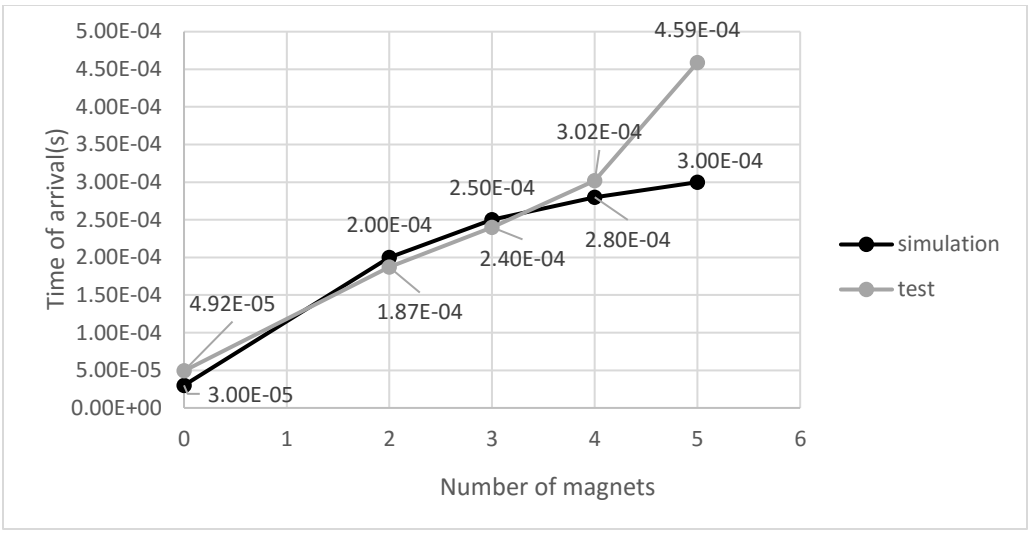

(a)

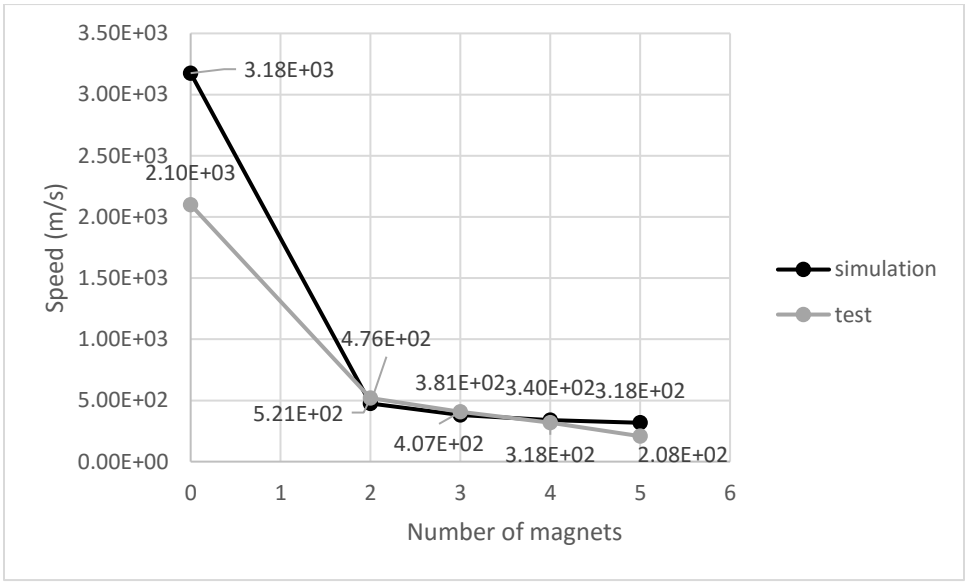

(b)

Figure 30. Test 3 results comparison of (a) time of arrival (b) wave speed

Both experimental results and numerical simulation results show that the masses have a significant influence on wave propagation and generated signals, time of arrival and wave speed changes with the number of magnets. Distance between laser hitting point and

sensor is also a factor that only affect the time of arrival. As long as the medium in wave propagation path do not change, wave speed will keep constant.

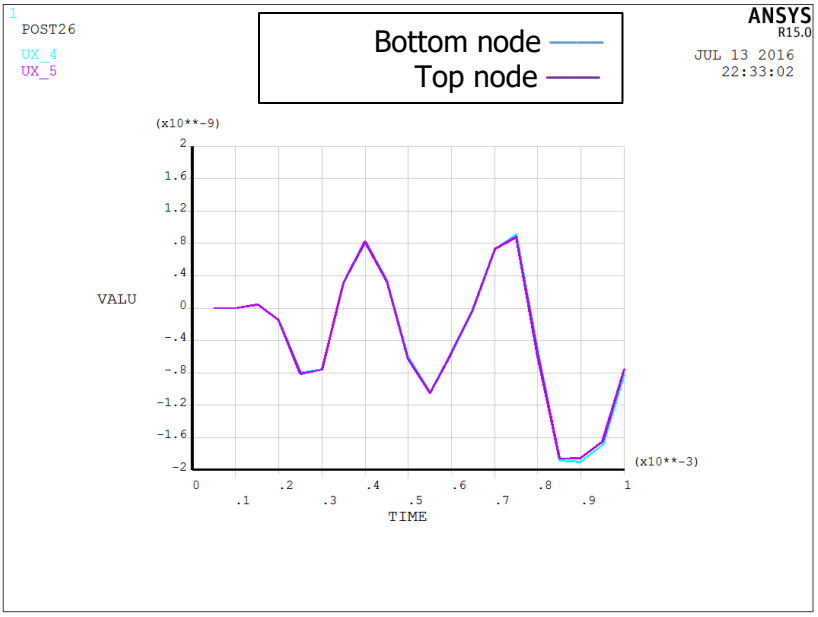

(a)

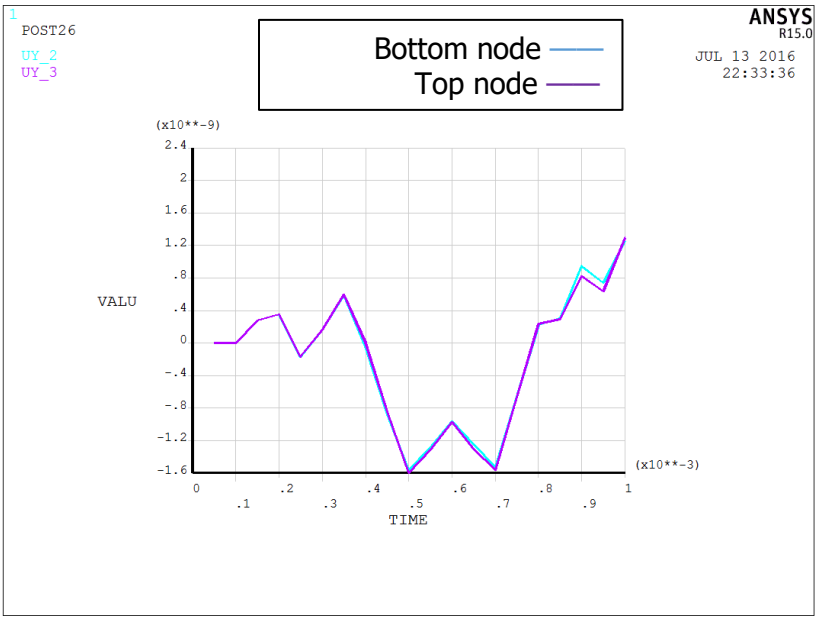

(b)

Figure 31. Extracted (a) x displacement (b) y displacement of the simulation

Wave mode study was also discussed in this paper. Temperature loading function applied on the surface of the laser hitting point, both symmetric and anti-symmetric modes were simulated[26], waveforms from the top node and bottom node could be obtained in Fig. 31. The displacement in x direction vs. time shows in figure (a) and the relationship between displacement in y direction and time shows in figure (b). From these two figures, waveforms of top node and bottom node are perfectly fit, therefore, the dominant Lamb wave mode is S_0 mode, which is the symmetric mode.

Chapter 4

CONCLUSIONS

An integrated experimental and simulation framework for a novel optoacoustic wave generation for damage detection in structural materials is developed. Several major conclusions can be drawn based on the proposed study.

- Both numerical simulation and experimental testing show the feasibility using a low-power high-frequency MOPA laser to generate acoustic wave in structural materials;
- The proposed methodology is sensitive to the local mass change and have the potential for the future implementation for small damage detection;
- The noise level is high due to the use of low power laser source and the proposed filtering and Hilbert-Huang transformation is shown to be able to extract the time of arrival information accurately;
- Certain experimental parameters, especially the laser firing parameters have significant effect on the generated signals. The current setup shows a 100kHz pulse frequency with 200ns pulse duration can generate clear acoustic wave signals in thin aluminum plate.

Significant future numerical and experimental studies are required. Some of them are listed below.

- Large noise exists in the proposed methodology and future noise reduction techniques (both hardware and software) are required for more accurate analysis;
- Automated scanning for large area detection is also needed with additional instrumentation development;

- Inverse imaging reconstruction algorithms using the developed technique needs to be developed and validated;
- Extension of the proposed method to composite materials is desired.

REFERENCES

[1] K. Dragan, M. Dziendzikowski, T. Uhl, and L. Ambrozinski, “Damage detection in the aircraft structure with the use of integrated sensors - SYMOST project,” *Proc. 6th Eur. Work. - Struct. Heal. Monit. 2012, EWSHM 2012*, vol. 2, pp. 974–980, 2012.

[2] R. Mohan and M. Mitra, “Lamb Wave Based Tomography for Damage Detection in Aluminium Plate,” no. November, pp. 3–4, 2011.

[3] A. Klepka, T. Uhl, T. Stepinski, L. Ambrozinski, and J. Ochonski, “Comparison of Two Baseline-Free Damage Detection Techniques Based on Lamb Waves Propagation Phenomena,” *Signserv.Teknikum.Uu.Se*.

[4] F. Li, H. Murayama, K. Kageyama, and T. Shirai, “Guided wave and damage detection in composite laminates using different fiber optic sensors,” *Sensors*, vol. 9, no. 5, pp. 4005–4021, 2009.

[5] W. Ostachowicz, T. Wandowski, and P. Malinowski, “Damage Detection Using Laser Vibrometry,” *NDT Aerosp.*, pp. 1–8, 2010.

[6] M. Ruzzene, “Frequency-wavenumber domain filtering for improved damage visualization,” *AIP Conf. Proc.*, vol. 894, pp. 1556–1563, 2007.

[7] R. B. Jenal, W. J. Staszewski, and A. Klepka, “Structural Damage Detection Using Laser Vibrometers,” *NDT Aerosp.*, pp. 1–8, 2010.

[8] S. E. Burrows, B. Dutton, and S. Dixon, “Laser generation of lamb waves for defect detection: Experimental methods and finite element modeling,” *IEEE Trans. Ultrason. Ferroelectr. Freq. Control*, vol. 59, no. 1, pp. 82–89, 2012.

[9] S. Yashiro, N. Toyama, J. Takatsubo, and T. Shiraishi, “Laser-Generation Based Imaging of Ultrasonic Wave Propagation on Welded Steel Plates and Its Application to Defect Detection,” *Mater. Trans.*, vol. 51, no. 11, pp. 2069–2075, 2010.

[10] M. Ochiai, “Development and Applications of Laser-ultrasonic Testing in Nuclear Industry,” *Int. Symp. Laser Ultrason. Sci. Technol. Appl.*, vol. Science, T, no. March, pp. 4–12, 2008.

[11] R. F. Anastasi, A. D. Friedman, and M. K. Hinders, “APPLICATION OF LASER BASED ULTRASOUND FOR NDE OF DAMAGE IN THICK STITCHED COMPOSITES,” 1997.

[12] G. Diot, A. Koudri-David, H. Walaszek, S. Guégan, and J. Flifla, “Non-destructive testing of porosity in laser welded aluminium alloy plates: Laser ultrasound and frequency-bandwidth analysis,” *J. Nondestruct. Eval.*, vol. 32, no. 4, pp. 354–361, 2013.

[13] Y.-K. An, B. Park, and H. Sohn, “Complete noncontact laser ultrasonic imaging for automated crack visualization in a plate,” *Smart Mater. Struct.*, vol. 22, no. 2, p.

025022, 2013.

[14] C. Zhang, J. Qiu, and H. Ji, “Laser Ultrasonic Imaging for Impact Damage Visualization in Composite Structure,” *EWSHM - 7th Eur. Work. Struct. Heal. Monit.*, 2014.

[15] L. Mallet, B. C. Lee, W. J. Staszewski, and F. Scarpa, “Structural health monitoring using scanning laser vibrometry: II. Lamb waves for damage detection,” *Smart Mater. Struct.*, vol. 13, no. 2, pp. 261–269, 2004.

[16] S. E. Burrows, S. Dixon, S. G. Pickering, T. Li, and D. P. Almond, “Thermographic detection of surface breaking defects using a scanning laser source,” *NDT E Int.*, vol. 44, no. 7, pp. 589–596, 2011.

[17] B. Xu, Z. Shen, J. Wang, X. Ni, J. Guan, and J. Lu, “Thermoelastic finite element modeling of laser generation ultrasound,” *J. Appl. Phys.*, vol. 99, no. 3, 2006.

[18] P. Rafiee, M. Lederer, and G. Khatibi, “Non-destructive damage detection using a scanning laser doppler vibrometer and the correlation method,” pp. 211–220, 2012.

[19] a C. Okafor and A. Dutta, “Structural damage detection in beams by wavelet transforms,” *Smart Mater. Struct.*, vol. 9, pp. 906–917, 2000.

[20] C. T. Ng and M. Veidt, “A Lamb-wave-based technique for damage detection in composite laminates,” *Smart Mater. Struct.*, vol. 18, no. 7, p. 074006, 2009.

[21] P. Soltani and N. Akbareian, “Finite element simulation of laser generated ultrasound waves in aluminum plates,” *Lat. Am. J. Solids Struct.*, vol. 11, no. 10, pp. 1761–1776, 2014.

[22] J. Ju and S. Ma, “Thermal Analysis of High Power Pulse Laser Module.”

[23] A. Soni and R. K. Patel, “Two Dimensional Finite Element Modeling Of Single Pulse Laser Drilling,” vol. 2, no. 3, pp. 389–396, 2013.

[24] S. Safdar, L. Li, M. A. Sheikh, and Zhu Liu, “Finite element simulation of laser tube bending: Effect of scanning schemes on bending angle, distortions and stress distribution,” *Opt. Laser Technol.*, vol. 39, no. 6, pp. 1101–1110, 2007.

[25] N. E. Huang and Z. Wu, “a Review on Hilbert-Huang Transform : Method and Its Applications,” *October*, vol. 46, no. 2007, pp. 1–23, 2008.

[26] T. Peng, a. Saxena, K. Goebel, Y. Xiang, and Y. Liu, “Integrated experimental and numerical investigation for fatigue damage diagnosis in composite plates,” *Struct. Heal. Monit.*, vol. 13, no. 5, pp. 537–547, 2014.